

## A route for the direct crystallization of dolomite† ‡

JUAN DIEGO RODRIGUEZ-BLANCO<sup>1,2</sup>, SAMUEL SHAW<sup>3</sup> AND LIANE G. BENNING<sup>1,4,\*</sup>

<sup>1</sup>School of Earth and Environment, University of Leeds, Leeds LS2 9JT, U.K.

<sup>2</sup>Nano Science Center, Department of Chemistry, University of Copenhagen, 2100 Copenhagen, Denmark

<sup>3</sup>School of Earth, Atmospheric and Environmental Sciences, The University of Manchester, Oxford Road, Manchester M13 9PL, U.K.

<sup>4</sup>GFZ German Research Centre for Geosciences, Telegrafenberg, D-14473 Potsdam, Germany

### ABSTRACT

The direct crystallization of dolomite from an aqueous solution at temperatures between 60–220 °C was followed in situ through time-resolved synchrotron-based energy-dispersive X-ray diffraction combined with offline high-resolution imaging, X-ray diffraction, and infrared spectroscopy. Crystalline CaMg(CO<sub>3</sub>)<sub>2</sub> phases form through a three-stage process. In the first stage, a nanoparticulate magnesium-deficient, amorphous calcium carbonate (Mg-ACC) with a nominal formula of Ca<sub>0.606</sub>Mg<sub>0.394</sub>CO<sub>3</sub>·1.37H<sub>2</sub>O forms. After a temperature-dependent induction time, during stage 2 the Mg-ACC partially dehydrates and orders prior to its rapid (<5 min) crystallization to non-stoichiometric proto-dolomite. This occurs via the dissolution of Mg-ACC, followed by the secondary nucleation of proto-dolomite from solution. The proto-dolomite crystallization proceeds via spherulitic growth that follows a growth front nucleation mechanism with a de-novo and continuous formation of nanocrystalline proto-dolomite subunits that form spherical aggregates. In stage three of the reaction, the proto-dolomite transforms to highly crystalline and stoichiometric dolomite on a much longer timescale (hours to days), via an Ostwald-ripening mechanism. Such a three-stage crystallization can explain microbially induced proto-dolomites observed in modern hypersaline settings and may also be the route by which the Cryogenian cap dolomite deposits of the Neoproterozoic formed.

**Keywords:** Dolomite, proto-dolomite, spherulitic growth, amorphous calcium carbonate

### INTRODUCTION

Dolomite, CaMg(CO<sub>3</sub>)<sub>2</sub>, is one of the most common carbonate minerals in the geologic record (Machel 2004) and the most oversaturated carbonate mineral in the modern ocean (Tucker and Wright 1990). However, dolomite rarely forms in modern environmental systems (MacKenzie and Andersson 2013), which has led to considerable interest in understanding its formation pathway. There are two main mechanisms by which dolomite can form in the natural environment: (1) “directly from solution” or primary dolomite, and (2) dolomites that formed during diagenesis or burial, most often through secondary replacement (dolomitization) of previously precipitated calcite or aragonite (Machel 2004; Mckenzie and Vasconcelos 2009). The largest dolomite deposits in the geologic record (Machel 2004) are in the Phanerozoic and are diagenetic in origin. In modern environments dolomite currently forms through the “direct” route, but only in a restricted number of hypersaline environments [i.e., evaporitic lakes or sabkhas; e.g., Jones (1965), Lindtke et al. (2011), Meister et al. (2011)]. In such settings, microbial metabolic processes (predominantly sulfate reduction or methanogenesis) induce high alkalinity. Together with the moderate to high Mg:Ca concentration ratios (1:1 to 100:1), this creates high supersaturation levels that commonly lead to the formation

of “dumbbell shaped” aggregates of dolomite (Warthmann et al. 2000; Sánchez-Román et al. 2011). A similar “direct” formation mechanism, which also produces a radial growth morphology, has been suggested for dolomite cements in Cryogenian (~850 to ~650 Mya) reef carbonates (Hood et al. 2011; Hood and Wallace 2012). The presence of directly precipitated dolomite cements during this period, has led to the oceans being classified as “aragonite-dolomite-seas.” In contrast the Phanerozoic oceans are classified as “calcite-aragonite seas” (Sandberg 1983), with the abundant dolomite found in Phanerozoic sediments having formed via various diagenetic and burial processes, but not through direct precipitation from seawater. The switch from dominantly “direct” dolomite formation to indirect “dolomitization” as the formation pathway may be related to the changes in ocean chemistry over time. The abundance of dolomite in the Phanerozoic, yet its scarcity in modern systems is not easily explained because we lack a fundamental understanding of how low-temperature dolomites form in marine settings and whether such formation reactions lead to primary or early secondary diagenetic dolomites. This has led to the paradox termed the “Dolomite Problem,” which is a long-standing debate with important mineralogical and palaeo-environmental implications, as it links the formation of dolomite with the long-term evolution of Earth’s ocean chemistry. However, there are key knowledge gaps in this field, which limit a thorough interpretation of dolomite formation in the geological record. One of these is a lack of a mechanistic understanding of the “direct” dolomite formation

\* E-mail: L.G.Benning@leeds.ac.uk

† ‡ Open access: Article available to all readers online.

pathway, and the factors (e.g., temperature, supersaturation, etc.) that may favor or inhibit this process.

This is particularly relevant because, as yet, inorganic dolomite has not been synthesized at ambient conditions directly from solution (Land 1998). Most experimental inorganic dolomite formation studies have quantified the “dolomitization” of calcite (Gaines 1977; Katz and Matthews 1977; Miura and Kawabe 2000; Nordeng and Sibley 1994; Kaczmarek and Sibley 2007), other Ca-Mg carbonates (Katz and Matthews 1977; Zempolich and Baker 1993; Sibley et al. 1994), or followed proto-dolomite crystallization (Malone et al. 1996) or dolomite growth (Gaines 1977; Arvidson and Mackenzie 1999; Higgins and Hu 2005; Hu et al. 2005, 2006) on various carbonate seed crystals. These experiments all mimic the diagenetic dolomite formation processes. Only a few experimental studies have attempted to quantify the fundamental reactions controlling the formation of inorganic dolomite “directly” from solution (Ohde and Kitano 1978; Kelleher and Redfern 2002; Schmidt et al. 2005). These inorganic experiments showed that a crystalline carbonate [but typically not stoichiometric  $\text{CaMg}(\text{CO}_3)_2$ ] formed from an amorphous Ca-Mg carbonate precursor. This precursor precipitated from highly supersaturated solutions, and transformed to dolomite via proto-dolomite at moderate to high temperatures (e.g., 40–200 °C; Kelleher and Redfern 2002; Schmidt et al. 2005). Proto-dolomite has no ordering of Mg and Ca within its structure and often forms micrometer-sized spheres made up of aggregates of small particles (<200 nm; e.g., Malone et al. 1996). Such proto-dolomites are usually distinguished from crystalline dolomite by the lack of superstructure peaks in the powder diffraction pattern (Kelleher and Redfern 2002). Malone et al. (1996) showed that at 50–200 °C and over long time periods proto-dolomite transforms to crystalline dolomite via a dissolution and reprecipitation reaction. This transformation lead to dolomite crystals with well developed crystallographic faces, but significant crystallographic ordering of the Ca and Mg was only achieved at 200 °C. Several microbial studies (e.g., Kenward et al. 2009; Sánchez-Román et al. 2011) have also shown the formation of proto-dolomite and dolomite at ambient conditions, but it is unclear whether an amorphous carbonate precursor formed prior to crystallization. These inorganic and microbial studies have conceptually described the multi-step crystallization of proto-dolomite and dolomite, however, the mechanisms by which these reactions take place have not yet been quantified.

Comparing the direct dolomite formation pathway with that of calcite also from an amorphous precursor (amorphous calcium carbonate, ACC) reveals many similarities. Magnesium-free ACC crystallizes rapidly to vaterite via spherulitic growth (Bots et al. 2012), followed by the slower transformation of vaterite to calcite via dissolution and re-precipitation (Rodriguez-Blanco et al. 2011). Spherulitic crystal growth is common in various systems [e.g., polymers supercooled from a molten state, Keith and Padden (1963); crystallization of viscous magmas, Lofgren (1971); see also review of Shtukenberg et al. (2012) and references therein]. Spherulitic growth has been shown to proceed via a growth front nucleation mechanism (Gránásky et al. 2005; Shtukenberg et al. 2012), which requires a high crystallization driving force (i.e., high supersaturation) that leads to the formation of spherical nanocrystal aggregates. For the

carbonate system it has been demonstrated that the amorphous ACC precursor transforms to vaterite via spherulitic growth (Beck and Andreassen 2010; Andreassen et al. 2010; Bots et al. 2012), and that this reaction occurs at high superaturations and leads to spheroidal vaterite aggregates. Interestingly, such spheroidal morphologies are similar to those observed for proto-dolomite/dolomite formed in microbial systems (i.e., spheroidal or dumbbell-shaped dolomite aggregates) suggesting that microbially induced Ca-Mg-carbonates may have also formed via spherulitic growth (Warthmann et al. 2000; Sánchez-Román et al. 2011). Furthermore, the radial growth morphology of the “direct” dolomite cements in the Neoproterozoic cap carbonates may also be a product of spherulitic growth indicating that they also may have formed from an amorphous precursor (Hood et al. 2011; Hood and Wallace 2012).

Thus, we hypothesize that an amorphous precursor is a necessary prerequisite for the crystallization of proto-dolomite/dolomite and that the spherulitic crystal growth mechanism observed in the pure  $\text{CaCO}_3$  system also controls the “direct” formation of proto-dolomite and dolomite in the Mg-Ca- $\text{CO}_3$  system. To address this we characterized the crystallization of an amorphous Ca-Mg carbonate precursor that was precipitated from a supersaturated, aqueous Ca-Mg carbonate solution with time via both conventional and in situ, time-resolved synchrotron-based methods. We then used these data to derive kinetic and mechanistic information for the nucleation, growth, and/or crystallization of proto-dolomite and dolomite. We did this to address three primary questions: (1) what is the mechanism of proto-dolomite formation from the amorphous precursor; (2) what is the mechanism of proto-dolomite transformation to crystalline dolomite; and (3) what are the key factors (e.g., saturation states, temperature), which control these mineral formation and crystallization reactions. The answers to these questions will provide a mechanistic basis for the crystallization pathway for the direct proto-dolomite and dolomite formation in both modern and ancient systems, e.g., microbially mediated proto-dolomite formation in sabka environments and Cryogenian reef dolomites of the Neoproterozoic.

## EXPERIMENTAL METHODS

Experiments were carried out by mixing 1, 1.5, or 2.5 M  $\text{Na}_2\text{CO}_3$ ,  $\text{CaCl}_2$ , and  $\text{MgCl}_2$  solutions (ratio of  $\text{CO}_3^{2-}:\text{Ca}^{2+}:\text{Mg}^{2+} = 2:1:1$ ) at room temperature in a stirred, polytetrafluoroethylene-lined hydrothermal reaction cell. Crystallization was then induced by heating the sealed cells to temperatures between 25 and 220 °C for between 30 min and 10 days. Mixing the starting solutions induced the instantaneous formation of a white, gel-like precipitate. The transformation of this white gel was followed online with synchrotron-based diffraction and offline with conventional techniques. The changes in the reaction cell contents were monitored in situ and in a time resolved manner via changes in energy-dispersive X-ray diffraction (ED-XRD) patterns collected on the white-beam station 16.4 at the Synchrotron Radiation Source (SRS), Daresbury Laboratory, U.K. At temperatures between 60 and 220 °C, ED-XRD scans of the crystallizing gel were recorded at 1 min intervals to follow the formation and changes in Bragg peak intensities throughout each reaction for up to 2 h. The reactions were considered complete when the intensity of all Bragg peaks stopped increasing. The ED-XRD patterns were fitted using XFIT (Cheary and Coelho 1992) and the peak areas and the overall background intensity as a function of time calculated and normalized to values between 0 and 1 to express the degree of reactions ( $\alpha$ ). The increase in peak area with time from each experiment was fitted to various crystallization kinetic models (Johnson and Mehl 1939; Bischoff and Fyfe 1968; Ogino et al. 1990) to derive the kinetic parameters. More detailed descriptions of the online, in situ experimental protocols and data analyses procedures can be found in Cahill et al. (2000), Shaw et al. (2005), and

Davidson et al. (2008).

In equivalent offline experiments (with no ED-XRD data collection) the white gel-like precipitate was reacted at 25–220 °C for up to 6 h (1 M initial concentrations) and at 25 to 60 °C for up to 10 days (1, 1.5, and 2.5 M initial concentrations). These offline experiments were quenched and separated from the aqueous solutions by vacuum-filtration (0.2 µm polycarbonate Cyclopore filters) and the solids (initial gel, intermediates, and end-products) were dried with isopropanol following the procedure described in Rodriguez-Blanco et al. (2008). These solids were analyzed with powder X-ray diffraction using a Bruker D8 powder X-ray diffractometer fitted with a GE (111) monochromator (PXRD,  $\text{CuK}\alpha_1$ ,  $\lambda = 1.541 \text{ \AA}$ ;  $2\theta = 5\text{--}70^\circ$ ;  $0.001^\circ$  step size; 0.5 s dwell time/step). In all cases, a silicon internal standard (Aldrich; ICDD PDF 27-1402) was used for  $2\theta$  calibration. From the PXRD patterns, the molar fraction of  $\text{MgCO}_3$  ( $\chi_{\text{MgCO}_3}$ ) in each crystalline end product was determined using the expression from Arvidson and Mackenzie (1999)

$$\chi_{\text{MgCO}_3} = \frac{M_{\text{MgCO}_3}}{M_{\text{MgCO}_3} + M_{\text{CaCO}_3}} = -3.6396d_{(104)} + 11.0405 \quad (1)$$

where  $M_{\text{MgCO}_3}$  and  $M_{\text{CaCO}_3}$  correspond to the moles of  $\text{MgCO}_3$  and  $\text{CaCO}_3$  per formula unit of dolomite, and  $d_{(104)}$  corresponds to the  $d$ -spacing ( $\text{\AA}$ ) of the (104) reflection of dolomite. To determine the magnesium content in the initial white gel-like precipitate, nine replicates of the gel were dried and digested in HCl and the calcium and magnesium concentration analyzed by ion chromatography following Bots et al. (2011). To discriminate between the proto-dolomite and dolomite, high-resolution PXRD scans ( $0.001^\circ$  step size; 2 s dwell time/step) of the offline reaction end products were acquired over the  $2\theta$  range between 20 to  $45^\circ$ . This way the low-intensity ( $\sim 1\%$ ) dolomite superstructure reflections, (101) and (015) were distinguishable (Goldschmidt et al. 1961; Arvidson and Mackenzie 1999). Finally, from these PXRD patterns, crystallite sizes were calculated via the Scherrer equation (Scherrer 1918) using the software code TOPAS (Coelho 2006).

The vibrational characteristics of the solids were also analyzed using an A2-Technology MicroLab mid-infrared spectrometer, with a diamond internal reflection sampling system. Spectra between 650 to  $4000 \text{ cm}^{-1}$  were accumulated by co-adding 512 scans with a  $4 \text{ cm}^{-1}$  resolution and spectral manipulation including baseline adjustment, normalization, and band component analysis was carried out using the Thermo-Nicolet OMNIC ESP 5.1 software package.

High-resolution photomicrographs of the solids were acquired using a field emission gun scanning electron microscope (FEG-SEM, LEO 1530 Gemini at 3 keV). From the FEG-SEM images, the particle size distributions in the white gel like precursor phase and the crystalline end products were determined by measuring the diameters of  $\sim 100$  particles each in representative images. It should be noted that due to the small size of some of the particles ( $< 50 \text{ nm}$ ) the measurement error from FEG-SEM image evaluations can reach 30%. The water content of the precursor phase was determined by thermogravimetric analyses (Mettler Toledo TGA/DSC1 Thermal Analyzer,  $10^\circ/\text{min}$  ramp between 30 and  $800^\circ\text{C}$ ) of 2 aliquots of the isopropanol-quenched starting material.

Last, the saturation indexes (SI) of the initial gel-like precipitate and the crystalline proto-dolomite and dolomite were calculated using the geochemical code PHREEQC (Parkhurst 1995) where the SI is defined as

$$\text{SI} = \log \frac{a_{\text{Ca}^{2+}} \cdot a_{\text{Mg}^{2+}} \cdot (a_{\text{CO}_3^{2-}})^2}{K_{\text{sp}}} \quad (2)$$

with  $a$  corresponding to the activity of the  $\text{Ca}^{2+}$ ,  $\text{Mg}^{2+}$ , and  $\text{CO}_3^{2-}$  ions at various times of the reaction and  $K_{\text{sp}}$  corresponding to the solubility product of either dolomite or proto-dolomite (Robie et al. 1978; Carpenter 1980). To calculate the aqueous Ca and Mg concentrations after the formation of the initial gel-like precipitate, we assumed that the solubility of the initial Mg-rich gel was similar to pure amorphous calcium carbonate precursors (ACC; solubility from Brečević and Nielsen 1989). This was based on our own solid analysis and comparing with other carbonate studies in the literature (Davis et al. 2000). This way the aqueous post-gel precipitation solution composition (e.g.,  $\text{Ca}^{2+}$  and  $\text{Mg}^{2+}$ ) could be calculated using the initial aqueous ion concentrations (0.250 M  $\text{CaCl}_2$ , 0.250 M  $\text{MgCl}_2$ , and 0.500 M  $\text{Na}_2\text{CO}_3$ ), the ACC

solubility and the analyzed composition and water content of the initial gel-like precipitate. Full details of the modeling methodology and the assumptions made in this process are available in the Supplementary Information<sup>1</sup>.

## RESULTS

Offline PXRD analysis of the white gel-like phase that formed immediately upon mixing of the starting supersaturated solutions revealed broad diffraction peaks centered at approximately  $30^\circ$ ,  $45^\circ$ , and  $63^\circ 2\theta$  (Fig. 1, bottom pattern, marked with \*) indicating that the initial phase was poorly ordered. The position and width of these peaks are equivalent to those observed for amorphous calcium carbonate (ACC, Rodriguez-Blanco et al. 2008). The magnesium content in the precursor formed by mixing the 1 M solutions (ionic strength of 2.0) was measured to be  $\chi_{\text{MgCO}_3} = 0.394 (\pm 0.005; n = 9)$ . We will refer hereafter to this precursor phase as Mg-ACC, following the notation of Günther et al. (2005). TGA analyses of our Mg-ACC revealed a water content of  $1.37 \pm 0.04 \text{ mol per mole of Mg-ACC}$  (Table 1). Combining the  $\chi_{\text{MgCO}_3}$  and water contents allowed us to calculate a  $\text{Ca}_{0.606}\text{Mg}_{0.394}\text{CO}_3 \cdot 1.37\text{H}_2\text{O}$  formula for our Mg-ACC. Based on PHREEQC modeling (Supplementary Information<sup>1</sup>), the Mg-ACC in our experiments precipitated from solutions with high-ionic strengths (1, 1.5, and 2.5 M) that were highly supersaturated with respect to all Ca-Mg-carbonate phases. For example, starting with 1 M solutions, the SI of ACC at  $25^\circ\text{C}$  was 4.02, while for proto-dolomite and dolomite the SI was 8.62 and 9.16, respectively. Once the Mg-ACC precipitated at  $25^\circ\text{C}$  the SI for proto-dolomite and dolomite dropped to 2.46 and 3.00, respectively (see text and Supplementary Table 1<sup>1</sup>).

The offline experiments at 60 to  $200^\circ\text{C}$ , with initial reactant concentrations of 1 M, showed that after 6 h the Mg-ACC crystallized (upper pattern in Fig. 1) to either proto-dolomite (60 and  $100^\circ\text{C}$ ) or dolomite ( $\geq 140^\circ\text{C}$ ). Dolomite was differentiated from proto-dolomite through the presence of the (101) and (015) superstructure peaks in the PXRD pattern (pDol and Dol in insets in Fig. 1). Analysis of the high-temperature reaction products ( $> 140^\circ\text{C}$ ) after 30 and 60 min revealed only proto-dolomite peaks, with the superstructure peaks absent. Between 1 and 6 h the growth of the superstructure peaks indicated the transformation from proto-dolomite to dolomite. The initial Mg-ACC ( $\chi_{\text{MgCO}_3, \text{Mg-ACC}} = 0.39$ ) transformed to a non-stoichiometric, slightly Mg-

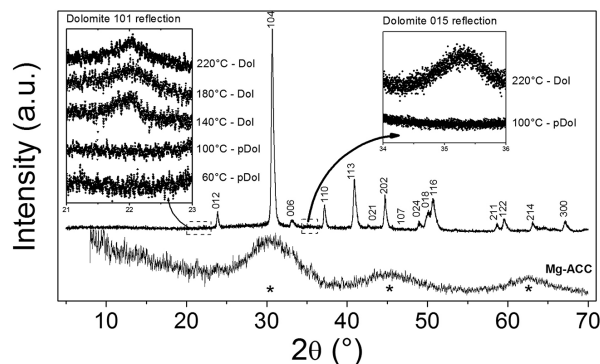


**FIGURE 1.** Powder X-ray diffraction patterns of Mg-ACC (lower pattern) and dolomite (upper pattern). The insets show the change in the (101) and the (015) reflections corresponding to the low-intensity superstructure peaks of dolomite.

<sup>1</sup> Deposit item AM-15-54963, Supplemental Material. Deposit items are stored on the MSA web site and available via the *American Mineralogist* Table of Contents. Find the article in the table of contents at GSW (ammin.geoscienceworld.org) or MSA (www.minsocam.org), and then click on the deposit link.

**TABLE 1.** Derived compositional, kinetic, and particle size parameters for the temperature-dependent crystallization of Mg-ACC

$T$ (°C)	$\chi_{\text{MgCO}_3}$ <sup>a</sup>	Crystallite size (nm) <sup>b</sup>	Nanoparticle/ nanocrystallite size (nm) <sup>c</sup>	$k$ (s <sup>-1</sup> ·10 <sup>-10</sup> )	$t_0$ (s)
25 (Mg-ACC)	0.394 ± 0.005 (n = 9)	–	44 ± 13	–	–
60	0.448(1)	23(5)	34 ± 9	6.50(4.43)	2790
100	0.437(1)	32(10)	34 ± 9	5.79(8.15)	2040
140	0.489(1)	69(28)	50–600	2.91(4.90)	650
180	0.494(2)	82(36)	50–600	9.15(1.97)	610
220	0.499(1)	139(63)	50–600	33.8(8.29)	580
Moles of H <sub>2</sub> O/mole of Mg-ACC	1.37 ± 0.04 (n = 2)				

Notes: For the molar fraction of MgCO<sub>3</sub> ( $\chi_{\text{MgCO}_3}$ ) (Eq. 1) and the crystallite sizes (Scherrer 1918) the standard deviations are shown in parentheses (error on last digit); for the conditional rate constant ( $k$ ), in parentheses shown are the fitting uncertainties ( $\pm 1\sigma$ ).

<sup>a</sup>  $\chi_{\text{MgCO}_3}$  was analyzed in the initial Mg-ACC and the solids reacted for 6 h at the given temperature.

<sup>b</sup> The Scherrer crystallite size was measured from PXRD patterns of the solids reacted for 6 h at the given temperature.

<sup>c</sup> Particle diameters were evaluated by measuring 100 particles in representative FEG-SEM images; the numbers refer to the nanoparticles in Mg-ACC and the crystalline subunits for proto-dolomite (60 and 100 °C) and dolomite (140, 180, and 220 °C).

deficient proto-dolomite ( $\chi_{\text{MgCO}_3, \text{pDol}} = 0.44\text{--}0.45$ ), which in turn transformed to a highly crystalline and stoichiometric dolomite ( $\chi_{\text{MgCO}_3, \text{Dol}} = \sim 0.50$ ; Table 1). In contrast at 60 °C, even after 10 days, proto-dolomite did not crystallize to dolomite. Furthermore, at lower temperatures (40 and 25 °C) and the same initial 1 M concentration, proto-dolomite did not form, instead the reaction products were monohydrocalcite (CaCO<sub>3</sub>·H<sub>2</sub>O) and minor (~5%) hydromagnesite [Mg<sub>5</sub>(CO<sub>3</sub>)<sub>4</sub>(OH)<sub>2</sub>·4H<sub>2</sub>O] (Supplementary Fig. 1<sup>1</sup>). When higher initial concentrations were used (i.e., 1.5 and 2.5 M), proto-dolomite formed at both 50 and 40 °C, yet at 25 °C again only monohydrocalcite and minor hydromagnesite (~5%) formed and both remained stable for long time periods (days).

Data from an in situ and time-resolved ED-XRD experiment of the crystallization of Mg-ACC at 180 °C is shown in Figure 2. At the start of the reaction a large background hump with no distinct diffraction peaks dominated. This background hump is a consequence of X-ray scattering from both the aqueous solution and the poorly ordered Mg-ACC. In all experiments, after a temperature-dependent induction period (Table 1) Bragg peaks at ~31° and 33° 2 $\theta$ , identified as the (104) and (006) proto-dolomite/dolomite peaks began to grow (Fig. 2). With increasing temperature, the induction time ( $t_0$ ) for the initiation of the crystallization reaction decreased from 48 min at 60 °C to 10 min at 220 °C (Fig. 3; Table 1). Once peaks started to grow, their intensity increased very rapidly (~5 min) and they reached their maximum intensity simultaneously, after which no further changes in intensities were observed. A distinction between dolomite and proto-dolomite was not possible using the ED-XRD data because the low resolution of the energy-dispersive detection system and large background signal from the solution did not allow the low-intensity superstructure peaks to be distinguished. The intensity of the background hump (Fig. 2) in the time resolved ED-XRD data decreased throughout the reaction. This decrease started prior to the formation of the Bragg peaks, and continued until the intensity of the peaks stopped increasing. For example, in the 180 °C experiment (Fig. 4), the first appearance of the (104) peak was observed after 10 min, when the intensity of the background hump had already decreased to  $\alpha = 0.5$ . At 15 min the Bragg peaks reached their maximum intensity while the background intensity reached a minimum.

The temperature-dependent crystallization of Mg-ACC described above was also confirmed by the changes in the FTIR spectra (Fig. 5). The spectra of Mg-ACC, proto-dolomite and dolomite all showed the characteristic bands for the carbonate ion

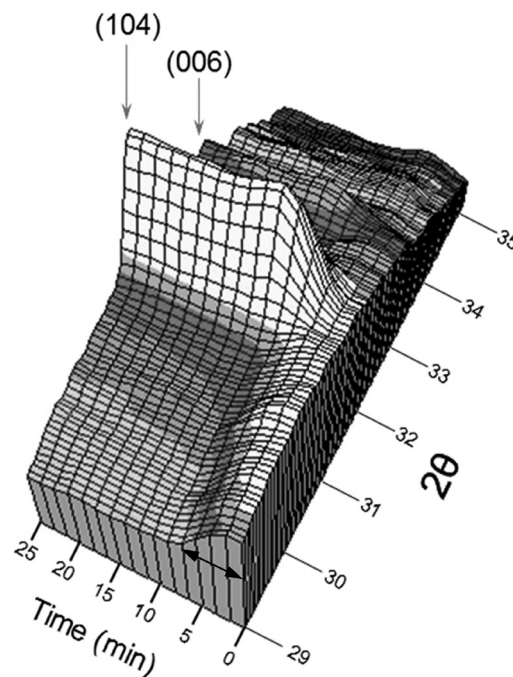


**FIGURE 2.** Three-dimensional representation of time-resolved ED-XRD patterns from the 180 °C experiment showing the formation of Bragg peaks identified as the (104) and (006) reflections for proto-dolomite/dolomite. For this plot energy has been converted to 2 $\theta$  using the Bragg equation ( $2d\sin\theta = n\lambda$ ) with  $\lambda = 1.541 \text{ \AA}$  (CuK $\alpha$ ).

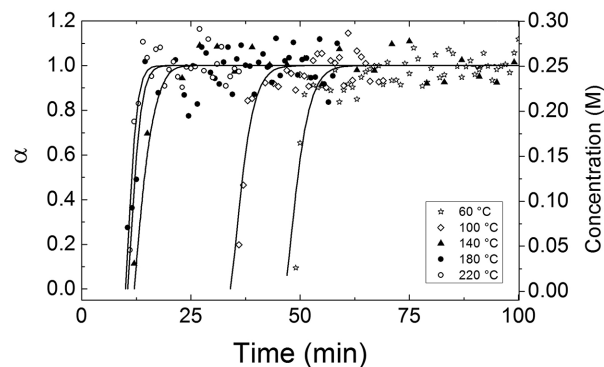


**FIGURE 3.** Degree of reaction ( $\alpha$ ) for the (104) reflection as a function of time and at five different temperatures. Solid lines indicate the fits to the first-order kinetic model (Eq. 3).

(symmetric and asymmetric  $\nu_x$  peaks for  $\text{CO}_3$ , Fig. 5) typical for most calcium and magnesium carbonates (Farmer 1974). However, similar to the spectrum for pure ACC (Günther et al. 2005; Rodriguez-Blanco et al. 2011), in the spectrum for the precursor Mg-ACC (bottom pattern in Fig. 5), the  $\nu_4$  symmetric in-plane bending vibration at  $725\text{ cm}^{-1}$  was absent. The presence of a sharp  $\nu_4$  vibration is normally an unambiguous signature for crystalline calcium or magnesium carbonates (upper pattern in Fig. 5; White 1974). The second clear distinguishing feature between the precursor Mg-ACC and the two crystalline phases was the presence of bands related to OH vibrations. These are the broad features centered around  $\sim 3300\text{ cm}^{-1}$ , corresponding to O-H stretching and the sharper band at  $1650\text{ cm}^{-1}$  corresponding to O-H bending vibrations, both are signatures for structural water. In the precursor Mg-ACC both these OH vibrations were prominent (bottom pattern in Fig. 5 and top spectra in inset), clearly showing that this phase was highly hydrated, also confirming the TGA data ( $\sim 1.4$  mol of water per mole of Mg-ACC). Upon

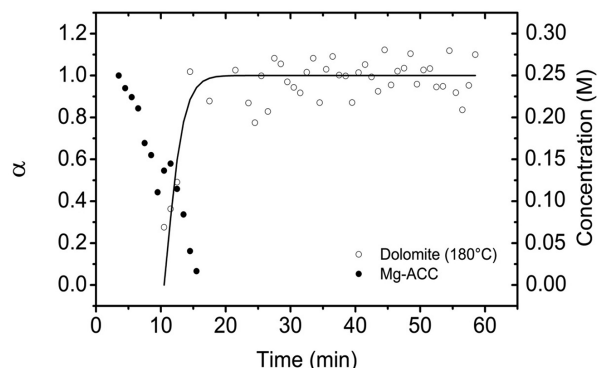


**FIGURE 4.** Degree of reaction ( $\alpha$ ) determined from the growth of the (104) reflection of dolomite and the change in background for Mg-ACC as a function of time at  $180^\circ\text{C}$ . Right-hand Y axis shows the moles of crystallized dolomite.

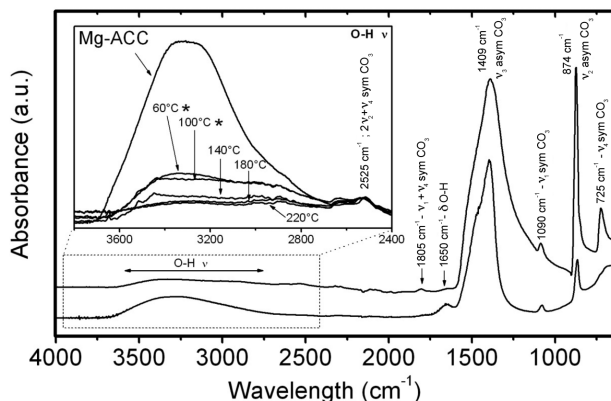


**FIGURE 5.** Fourier transform infrared spectra of Mg-ACC (bottom pattern) and crystalline (upper pattern) solids obtained at  $60$  to  $220^\circ\text{C}$ . The infrared bands from  $750$  to  $2600\text{ cm}^{-1}$  are identical for all solids except for the amorphous precursor, in which the  $725\text{ cm}^{-1}$  band is absent. The change in the degree of hydration as a function of temperature is evident in the inset.

crystallization to proto-dolomite and dolomite (upper pattern in main Fig. 5), the intensity of the broad OH-stretch and sharper OH-bend vibrations became weaker (inset in Fig. 5, normalized for comparison to the common  $2\nu_2 + \nu_4$  symmetric C-O vibration). The prominent OH band in the Mg-ACC spectra decreased as proto-dolomite partially dehydrated (marked with \* in inset Fig. 5), while dolomite was fully anhydrous (lower 3 patterns in inset Fig. 5).

The FEG-SEM images of the Mg-ACC revealed the presence of  $\sim 45\text{ nm}$   $\emptyset$  spherical nanoparticles (Fig. 6b; Table 1) that formed loose aggregates. These transformed to proto-dolomite (Figs. 6c and 6d) that were characterized by small, nanocrystals that coalesced into larger spheroidal aggregates or co-joined micrometer-sized hemispheres (Fig. 6c). The sizes of the nanocrystalline subunits in these larger proto-dolomite spheroids were smaller than the precursor Mg-ACC, and averaged  $\sim 35\text{ nm}$  (Fig. 6d; Table 1). Finally, the higher temperature dolomite formed larger spheres ( $\sim 5$ – $50\text{ }\mu\text{m}$ , Fig. 6d), but these were made up of larger ( $>50$  and  $<600\text{ nm}$ ) and highly crystalline subunits (Fig. 6f) characterized by idiomorphic crystal faces. The size of the individual subunits in the proto-dolomite and dolomite evaluated from the FEG-SEM images are similar to the

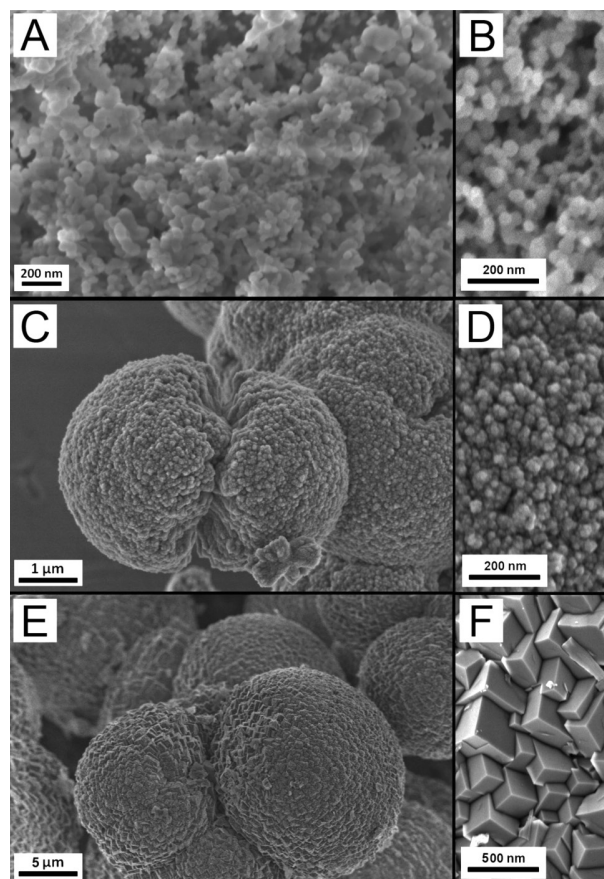


**FIGURE 6.** FEG-SEM images of the different solids that formed in the experiments: (a) precursor Mg-ACC nanoparticles; (c) proto-dolomite; and (e) dolomite. Images at right (b, d, f) show details of the Mg-ACC nanoparticles and the proto-dolomite and dolomite crystallite subunit sizes.

Scherrer crystallite sizes calculated from the PXRD data. These gradually increased from 23 nm for proto-dolomite formed at 60 °C to 139 nm for dolomite formed at 220 °C (Table 1).

## DISCUSSION

The results described above show that starting from super-saturated aqueous solutions can lead to the formation of dolomite via a three-stage reaction. The first stage is the fast precipitation of a poorly ordered, hydrated, and nanoparticulate precursor, Mg-ACC. In stage two, this precursor breaks down to form proto-dolomite, which ultimately transforms to dolomite in stage three. Each of these three stages and a detailed mechanistic evaluation of the reaction sequence are described below.

### Nature and stability of the Mg-ACC precursor

The formation of the Mg-ACC was instantaneous (within <1 s) in our experiments and thus its nucleation and growth were not evaluated in this study, we only characterized it and followed its crystallization. The PXRD and FTIR data for the Mg-ACC precursor phase are identical to those for ACC (Rodriguez-Blanco et al. 2008, 2011). The morphology (spherical) and size ( $44 \pm 13$  nm) of our starting Mg-ACC were also similar to that reported for ACC (e.g., Radha et al. 2010, sample ACC-5,  $\varnothing$  50–100 nm; Bots et al. 2012, ACC,  $\varnothing \sim 40$  nm). These suggest that our Mg-ACC is structurally similar to pure ACC. However, the  $\sim 1.4$  mol of water in our Mg-ACC are higher than the average 1 mol of water for pure ACC in the literature (Koga et al. 1998; Koga and Yamane 2008; Michel et al. 2008; Radha et al. 2012). Our data clearly links the high-Mg content in our starting Mg-ACC with the higher water content of our Mg-rich precursor when compared to pure ACC. This is also consistent with the recent study by Radha et al. (2012), who evaluated the crystallization energetics of various Mg containing ACC phases and inferred that a hydrated amorphous phase with a close to 0.5 Mg content is the least metastable and may be precursors for dolomite formation. This is linked with the fact that Mg is well known to have a significantly higher dehydration energy compared to calcium (Di Tommaso and de Leeuw 2010), and thus it is not surprising that it can retain more water when incorporated into the amorphous carbonate phase (Wang et al. 2009; Schmidt et al. 2005).

The decrease in background intensity in the time-resolved ED-XRD patterns to  $\sim 0.5$  (Fig. 4) prior to the appearance of any diffraction peak of proto-dolomite suggests that the Mg-ACC started transforming before the first proto-dolomite crystals grew. Studies of both inorganic and biogenic ACC have shown that an initial hydrated and highly disordered ACC (i.e., ACC with low-structural order) forms from solution and that this transforms to a less disordered and anhydrous ACC prior to crystallization (Gower 2008; Bots et al. 2012). Radha et al. (2010) showed that the thermodynamic stability (enthalpy) of less-disordered and anhydrous ACC is greater than that of more-disordered and hydrated ACC, therefore the dehydration and ordering of the ACC is likely to be thermodynamically driven (lowering of enthalpy in the system). We have shown that the initially hydrated and highly disordered Mg-ACC forms from solution and we suggest that this Mg-ACC gradually orders and may partially dehydrate prior to its crystallization, and that this likely occurs via a similar mechanism to that observed for pure ACC (Bots et al. 2012).

Less-disordered Mg-ACC has not been described previously but the dramatic decrease in background intensity in our ED-XRD patterns prior to its crystallization of proto-dolomite (Fig. 2) can be explained by the gradual formation of a more-ordered Mg-ACC. This is akin to the behavior observed for pure ACC (Radha et al. 2010; Bots et al. 2012) where prior to crystallization an increase in ordering of the amorphous phase was also likely accompanied by a lowering in water content and a final transformation to a fully anhydrous amorphous phase.

When compared to pure ACC, the current study showed that high concentrations of magnesium in the Mg-ACC dramatically delayed (300%) the onset of the crystallization. This is comparable to other studies where lower magnesium contents (10%) either delayed the crystallization onset (by up to 100%; Reddy and Nancollas 1976; Loste et al. 2003; Raz et al. 2003) or changed the crystallization pathway (Rodriguez-Blanco et al. 2012). For example, pure ACC, at ambient temperatures transforms within minutes to vaterite and subsequently to calcite (Rodriguez-Blanco et al. 2011), while 10% Mg in the ACC leads to a direct transformation to of the amorphous precursor to calcite with no vaterite intermediate but with a longer an induction time of  $\sim 15$  min (Rodriguez-Blanco et al. 2012).

Comparing these low-Mg-ACC transformation induction times to data in the current study shows that the high-Mg content in our Mg-ACC ( $\chi_{\text{MgCO}_3} = 0.39$ ) significantly increases the induction time of crystallization, allowing the poorly order Mg-ACC phase to remain stable for days at room temperature, and more than 30 min at 60 °C (Fig. 3). This is consistent with studies that showed a direct proportionality between Mg content and crystallization induction time in the calcium carbonate system (e.g., calcite formation; Reddy and Nancollas 1976; Tracy et al. 1998a, 1998b; Loste et al. 2003; Raz et al. 2003). This stabilizing effect of Mg in ACC can be attributed to the presence of hydrated Mg within the framework of the Mg-ACC nanostructure, which retards proto-dolomite nucleation due to its slow dehydration kinetics (Raiteri and Gale 2010; Jiang et al. 2010). We previously described a similar effect also in a system where the Mg content in the initial aqueous solution was lower [Rodriguez-Blanco et al. (2012); 10% of the aqueous  $\text{Ca}^{2+}$  was replaced with  $\text{Mg}^{2+}$ ] compared to the current study (50% of the aqueous  $\text{Ca}^{2+}$  was replaced with  $\text{Mg}^{2+}$  in this study). In Rodriguez-Blanco et al. (2012) we demonstrated that the presence of Mg delayed the formation of the first crystalline phase compared to the pure system (Rodriguez-Blanco et al. 2011) and also that direct calcite formation from the amorphous precursor was favored.

### Mechanism of formation for proto-dolomite

To derive the mechanism of crystallization for the precursor Mg-ACC our data offers various lines of evidence which include: the overall morphology, the crystallite size, the supersaturation, as well as the reaction rates all point to a spherulitic crystal growth mechanism for proto-dolomite. These will be now discussed in detail below.

First, the morphology of the proto-dolomite particles formed (i.e., spheroidal aggregates made up of nanocrystalline subunits) in all our experiments is indicative of a spherulitic growth mechanism (Andreassen 2005; Gránásky et al. 2005). Spherulitic growth of materials has been shown to occur in

many systems, via a nucleation-controlled growth process where the continuous nucleation of new particles on the surface of existing particles occurs via non-crystallographic branching (i.e., there is no structural relationship between the nucleating particle and that of the particle on which it has formed; Shtukenberg et al. 2012). This “secondary” process is usually termed “growth front nucleation” (Gránásy et al. 2005), and results in the formation of spherulites a few micrometers in size consisting of aggregated and fairly monodispersed nanoparticulate crystallites. Gránásy et al. (2005) argues that small changes in the nucleation process can lead to spherulites with various morphologies. These can be spheres (classified as category 1) or dumbbells (category 2). The growth morphology of the proto-dolomite in our study (co-joined micrometer-sized hemispheres consisting of aggregated nanoparticles) is consistent with “category 2” spherulites. However, morphological evidence on its own is not satisfactory to provide definitive confirmation for a spherulitic growth mechanism. Our second line of evidence supporting this mechanism is the high supersaturation with respect to proto-dolomite throughout our reaction. Once the Mg-ACC had precipitated after mixing of the initial highly supersaturated solutions, the SI for proto-dolomite was between 2.46 and 3.00 (at 25 and 220 °C, respectively, Supplementary Table 1<sup>1</sup>). Such a high supersaturation fosters a high crystallization driving force, which is another prerequisite for the continuous growth front nucleation process that controls spherulitic growth. Furthermore, the dissolution of minor amounts of Mg-ACC prior to the crystallization of proto-dolomite would increase the SI to higher levels, especially at higher temperatures (e.g., 220 °C) due to the reverse solubility of carbonates. As the reaction proceeds via a continual dissolution of the precursor Mg-ACC and the growth of proto-dolomite, the Mg-ACC is likely to be present until virtually all the proto-dolomite has formed, maintaining the high level of supersaturation throughout the spherulitic crystal growth reaction leading to proto-dolomite. Previous studies that followed the crystallization of calcium carbonates have shown that a saturation index >2–3 is required for spherulitic growth to occur. For example, in the case of the pure ACC to vaterite transformation that occurs also via spherulitic growth (Beck and Andreassen 2010; Andreassen et al. 2010; Bots et al. 2012) the SI for vaterite was usually equal or larger than 3.

The third line of evidence is the crystallization rate. Due to the nucleation-controlled growth mechanism, and the high level of supersaturation throughout the growth process, the formation rate during spherulitic growth is usually extremely rapid, relative to conventional surface controlled growth. The time resolved ED-XRD data indicates that the entire crystallization reaction is very rapid. Regardless of the temperature (60–220 °C) the complete crystallization occurred in ~5 min, which is consistent with the growth front nucleation process occurring during spherulitic growth. Finally, the nucleation controlled growth mechanism during spherulitic growth leads to the formation of nanoparticles, as very little, or no, surface growth occurs following nucleation. The average crystallite/particle sizes determined for the proto-dolomite in our experiments of between 23 and 34 (<100 °C, Table 1) are consistent with a nucleation dominated particle formation reaction. These particle sizes are comparable with the crystallite size for vaterite also formed via spherulitic

growth (~10 nm, Bots et al. 2012).

A kinetic model, which described the formation of three-dimensional spherulites via growth front nucleation, was derived by Gránásy et al. (2005). They indicate that the degree of reaction ( $\alpha$ ) for the crystallizing phase can be defined by the following equation

$$\alpha = 1 - e^{-[k(t-t_0)]^m} \quad (3)$$

where  $k$  ( $s^{-1}$ ) is the rate constant,  $t$  (s) is time,  $t_0$  (s) is the induction time. This kinetic model produced the best fit to the data for the growth of proto-dolomite obtained from the time-resolved ED-XRD data (Fig. 3; Table 1), and was a significantly better fit than any kinetic models for surface-controlled growth or simple chemical kinetics. This fit to the kinetic model for spherulitic growth provides additional evidence for this growth mechanism for proto-dolomite.

In summary, the overall morphology, the solution chemistry, crystallite sizes, as well as the derived kinetics for proto-dolomite formation all point to a spherulitic growth mechanism and no other crystallization mechanisms fits all the observations. This conclusion is consistent with previous studies of pure ACC crystallization in solution, which leads to the spherulitic growth of vaterite. However, this is the first study to show that proto-dolomite forms from Mg-ACC via the same spherulitic crystallization mechanism.

#### Proto-dolomite to dolomite transformation

The offline crystallization data indicated that following the spherulitic growth of proto-dolomite, a gradual transformation to dolomite occurred at temperatures >100 °C (Figs. 1 and 5). During this stage of the reaction no increase in PXRD peak intensities was observed (Figs. 2 and 4), suggesting no additional material formed. Malone et al. (1996) proposed that the transformation of proto-dolomite to ordered dolomite may involve multiple episodes of recrystallization and Ostwald-ripening. Kelleher and Redfern (2002) proposed Ostwald-ripening of a hydrous Ca-Mg carbonate phase (likely proto-dolomite) as the kinetic answer to the problem of dehydrating Mg to form ordered dolomite. This mechanism is consistent with the observation in this current study. The increase in crystallite and particle sizes (Table 1) and the development of well-defined crystal faces as proto-dolomite transforms to ordered dolomite, occurs via an Ostwald ripening, dissolution and reprecipitation mechanism. Ostwald ripening reactions occur when the supernatant solution is near saturation with respect to the crystallizing phase. This is in contrast to the very high level of saturation required for proto-dolomite spherulitic growth. Once all Mg-ACC crystallized to proto-dolomite via spherulitic growth, and the Ostwald ripening to ordered dolomite was initiated, the SI of the solution with respect to dolomite must have decreased dramatically due to its equilibration with the next most soluble phase, which is proto-dolomite. The small driving force required for the Ostwald ripening reaction is a consequence of the small difference in solubility between proto-dolomite and ordered dolomite. This second crystallization stage was slower than the spherulitic proto-dolomite growth (hours to weeks), but ultimately led to the formation of anhydrous and highly crystalline, euhedral dolomites with a stoichiometric Ca:Mg

composition (Table 1). Malone et al. (1996) also crystallized proto-dolomite to ordered dolomite and showed that below 100 °C, even after 336 days only 50% of his initial proto-dolomite had recrystallized, while above 100 °C, the recrystallization rates were higher but only reached 100% at 200 °C after 40 days. In his recrystallization experiments, Malone et al. (1996) regardless of temperature and time, only obtained ordered dolomite that was not non-stoichiometric. The temperature-dependent proto-dolomite to ordered dolomite transformation was confirmed in the current study, yet we obtained highly ordered and stoichiometric dolomites and obtained a full crystallization at much faster rates (i.e., >100 °C within 6 days). This difference is most likely a consequence of the variations in supersaturation levels during this stage of the reaction, which were higher in the current study compared to those in the Malone et al. (1996) study, who re-equilibrated his synthesized proto-dolomite with a new solution of seawater ionic strength. Nevertheless, both studies show a proto-dolomite to dolomite transition, which is driven by a surface dissolution and reprecipitation mechanism as also suggested by Kelleher and Redfern (2002).

## IMPLICATIONS

### How does the formation of proto-dolomite/dolomite from Mg-ACC compare to the crystallization of pure ACC?

The fast precipitation of Mg-ACC followed by spherulitic growth of proto-dolomite and ripening to dolomite is similar to the mechanism described for the pure calcium carbonate system. In the absence of magnesium, ACC transforms to vaterite via spherulitic growth and this subsequently ripens and re-crystallizes to calcite (Bots et al. 2012; Rodriguez-Blanco et al. 2011). Our initial hypothesis that an amorphous precursor is a prerequisite for the formation of proto-dolomite via spherulitic growth is correct. We further assert that the first crystalline phase to form from all compositions of ACC (with or without Mg) always occurs via a spherulitic growth mechanism. The prime reason for this universal process is the large difference in solubility between the ACC (or Mg-ACC of variable compositions) and all crystalline Mg-Ca-carbonate polymorphs. This spherulitic growth pathway has so far been documented for the crystallization of pure ACC (Andreassen 2005; Bots et al. 2012; Rodriguez-Blanco et al. 2011; Sand et al. 2012), for a 30% Mg-ACC precursor to monohydrocalcite (Rodriguez-Blanco et al. 2014) as well as in this study where the initial solutions contained 50% Mg. A comprehensive evaluation of the formation of other Ca/MgCO<sub>3</sub> phases from amorphous precursors needs to be undertaken to prove this hypothesis.

### Do our experimental results mimic the observed “direct” microbial mediated proto-dolomite/dolomite formation in modern hypersaline settings?

In such environments biogenic proto-dolomite forms at ambient to moderately high temperatures (e.g., alkaline lakes or shabkhas *T* between 27–50 °C), high alkalinities (up to 500 mM), and high-Mg:Ca concentration ratios (>1:1 to 100:1) (Folk and Land 1975; Last and De Deckker 1990; Meister et al. 2011 and references therein). These conditions lead to supersaturated conditions suitable for the precipitation of amorphous carbonates. Compar-

ing our experimental results with bacterially mediated dolomite formation studies (e.g., Kenward et al. 2009; Sánchez-Román et al. 2011; Meister et al. 2011), reveals many similarities including the resulting particle morphologies, the supersaturation/alkalinity and temperature. In our experiments, we showed that the reaction from the amorphous precursor to a first crystalline phase occurs in all cases via fast, secondary nucleation dominated crystallization. Such a reaction results in nanocrystalline particles that develop a spherulitic morphology, a shape that is akin to the “dumb-bells and cauliflower structures” described by McKenzie and Vasconcelos (2009) for bacterially mediated proto-dolomites. Thus we suggest that such a spherulitic growth mechanism is the controlling prerequisite for the formation of the intricately shaped biomineralized proto-dolomite and dolomite observed in modern hypersaline settings. In our inorganic experiments the initial amorphous Mg-ACC precipitates from solutions that were highly supersaturated with respect to proto-dolomite (SI > 8), while the saturation indexes for proto-dolomite and dolomite dropped to close to 3 once Mg-ACC had formed. Similarly, in bacterially mediated reactions, SI values of 3.36 were reported (Kenward et al. 2009) which are comparable to those reported here and by others for spherulitic growth carbonate systems (Andreassen 2005; Bots et al. 2012). Furthermore, our Mg-ACC only crystallized to proto-dolomite at temperatures >40 °C, yet in microbial systems proto-dolomite and dolomite have been shown to form at temperatures as low as 25 °C. This indicates that besides the high supersaturation and high alkalinity, another so far not understood factor has to affect the dolomite crystallization process. This factor may be the presence of organics. Zhang et al. (2012), based on their experiments with carboxymethyl cellulose and agar, suggested that extracellular polysaccharides produced by microorganisms could be key in the formation of proto-dolomite at ambient temperatures. Yet, based on the above described chemical as well as the morphological similarities (spheroidal nanocrystalline aggregates), our data indicates that in microbially mediated systems the initial formation of proto-dolomite must proceed via the same spherulitic transformation pathway of the amorphous precursor leading to proto-dolomite and then to dolomite via re-crystallization. We suggest that in bacterial systems dolomite forms due to the alkalinity produced by the microbial processes, and that the degree of order and also the Mg content in the resulting mineral phase increases from proto-dolomite to dolomite during ripening, both processes we have quantified in this current study for the inorganic system.

### Finally, what can we learn from our experimental results with regard to the inferred “direct” dolomite precipitation processes in ancient natural systems?

Hood et al. (2011) and Hood and Wallace (2012) suggest that the environmental conditions that dominated and promoted the “direct precipitation” of dolomite from solution in the Neoproterozoic seas were characterized by high alkalinities, elevated Mg:Ca ratios (>7) and high supersaturations. These conditions are similar to those in our experiments indicating that the dolomite cements most likely formed via the precipitation of an Mg-rich ACC, and its transformation to proto-dolomite via spherulitic growth as we have documented in this study. The Cryogenian dolomite cements were characterized by radially

shaped growth morphologies, similar to the spherical morphology observed in this study and in the microbial studies. We suggest that the radial morphology is a remnant of a cross section through spherulites formed during the spherulitic growth of proto-dolomite. This leads us to infer that if the assertion of a “direct” dolomite cement formation scenario is correct, the spherulitic growth mechanism could have been the controlling pathway to produce the Cryogenian cap dolomites described by Hood et al. (2011), regardless of whether their formation occurred via a microbially mediated processes as suggested by Font et al. (2010).

Overall, our combined data sets showed that the occurrence, structure, composition, hydration, and morphology of proto-dolomite and dolomite can be explained by a three-step process: (1) the precipitation of a highly hydrated, magnesium deficient, and amorphous carbonate precursor, Mg-ACC; (2) the dehydration of this Mg-ACC precursor and concomitant growth of the proto-dolomite via a spherulitic mechanism; and (3) the re-crystallization of proto-dolomite via Ostwald ripening to form dolomite. Our results also demonstrate that in biomineralization reactions, growth morphologies can be a consequence of spherulitic growth that is in turn promoted by high supersaturation. Last, our results have important palaeo-environmental implications as they shed light on the past ocean chemical conditions necessary for the formation of ancient dolomites in the geological record and help explain the formation of proto-dolomite/dolomite in modern settings.

#### ACKNOWLEDGMENTS

This research was supported by the Marie Curie EU-FP6 MIN-GRO Research and Training Network under contract MRTN-CT-2006-035488 and CCLRC beamtime award (Grant No. 50115 to Liane G. Benning). The authors would like to thank Dave Taylor from the Synchrotron Radiation Source, Daresbury Laboratory, U.K., for help during beamtime.

#### REFERENCES CITED

- Andreassen, J.P. (2005) Formation mechanism and morphology in precipitation of vaterite—Nano-aggregation or crystal growth? *Journal of Crystal Growth*, 274, 256–264.
- Andreassen, J.P., Flaten, E.M., Beck, R., and Lewis, A.E. (2010) Investigations of spherulitic growth in industrial crystallization. *Chemical Engineering Research and Design*, 88, 1163–1168.
- Arvidson, R.S., and Mackenzie, F.T. (1999) The dolomite problem: Control of precipitation kinetics by temperature and saturation state. *American Journal of Science*, 299, 257–288.
- Beck, R., and Andreassen, J.P. (2010) Spherulitic growth of calcium carbonate. *Crystal Growth and Design*, 10, 2934–2947.
- Bischoff, J.L., and Fyfe, W.S. (1968) Catalysis, inhibition and the calcite-aragonite problem. I. The aragonite-calcite transformation. *American Journal of Science*, 266, 65–79.
- Bots, P., Benning, L.G., Rickaby, R.E.M., and Shaw, S. (2011) The role of SO<sub>4</sub> in the switch from calcite to aragonite seas. *Geology*, 39, 331–334.
- Bots, P., Benning, L.G., Rodriguez-Blanco, J.D., Roncal-Herrero, T., and Shaw, S. (2012) Mechanistic Insights into the crystallization of amorphous calcium carbonate (ACC). *Crystal Growth and Design*, 12, 3806–3814.
- Brečević, L., and Nielsen, A.E. (1989) Solubility of amorphous calcium carbonate. *Journal of Crystal Growth*, 98, 504–510.
- Cahill, C.L., Benning, L.G., Barnes, H.L., and Parise, J.B. (2000) In situ time-resolved X-ray diffraction of iron sulfides during hydrothermal pyrite growth. *Chemical Geology*, 167, 53–63.
- Carpenter, A.B. (1980) The chemistry of dolomite formation: the stability of dolomite. In D.H. Zenger and J.B. Dunham, Eds., *Concept and Models of Dolomitization*. Society of Economic Paleontologists and Mineralogists Special Publication, 28, pp. 111–121.
- Cheary, R.W., and Coelho, A. (1992) A fundamental parameters approach to X-ray line-profile fitting. *Journal of Applied Crystallography*, 25, 109–121.
- Coelho, A. (2006) Topas-Academic, Coelho Software, Brisbane, Australia, <http://www.topas-academic.net>. Accessed March 25, 2012.
- Davidson, L.E., Shaw, S., and Benning, L.G. (2008) The kinetics and mechanisms of schwertmannite transformation to goethite and hematite under alkaline conditions. *American Mineralogist*, 93, 1326–1337.
- Davis, K.J., Dove, P.M., and De Yoreo, J.J. (2000) The role of Mg<sup>2+</sup> as an impurity in calcite growth. *Science*, 290, 1134–1137.
- Di Tommaso, D., and de Leeuw, N.H. (2010) Structure and dynamics of the hydrated magnesium ion and of the solvated magnesium carbonates: Insights from first principles simulations. *Physical Chemistry Chemical Physics*, 12, 894–901.
- Farmer, V.C. (1974) *Mineralogical Society Monograph 4: The Infrared Spectra of Minerals*. Mineralogical Society of Great Britain and Ireland. 539 pp.
- Folk, R.L., and Land, L.S. (1975) Mg/Ca ratio and salinity: Two controls over crystallization of dolomite. *American Association of Petroleum Geologist Bulletin*, 59, 60–68.
- Font, E., Nédélec, A., Trindade, R.I.F., and Moreau, C. (2010) Fast or slow melting of the Marinoan snowball Earth? The cap dolostone record. *Palaeogeography, Palaeoclimatology, Palaeoecology*, 295, 215–225.
- Gaines, A.M. (1977) Protodolomite redefined. *Journal of Sedimentary Petrology*, 47, 543–546.
- Goldschmidt, J.R., Graf, D.L., and Heard, H.C. (1961) Lattice constants of the calcium-magnesium carbonates. *American Mineralogist*, 46, 453–457.
- Gower, L.B. (2008) Biomimetic model systems for investigating the amorphous precursor pathway and its role in biomineralization. *Chemical Reviews*, 108, 4551–4627.
- Gránásky, L., Pusztai, T., Tegze, G., Warren, J.A., and Douglas, J.F. (2005) Growth and form of spherulites. *Physical Review Letters* E, 72, 011605.
- Günther, C., Becker, A., Wolf, G., and Eppler, M. (2005) In vitro synthesis and structural characterization of amorphous calcium carbonate. *Zeitschrift für anorganische und allgemeine Chemie*, 631, 2830–2835.
- Higgins, S.R., and Hu, X. (2005) Self-limiting growth on dolomite: Experimental observations with in situ atomic force microscopy. *Geochimica et Cosmochimica Acta*, 69, 2085–2094.
- Hood, A.v.S., and Wallace, M.W. (2012) Synsedimentary diagenesis in a Cryogenian reef complex: Ubiquitous marine dolomite precipitation. *Sedimentary Geology*, 255–256, 56–71.
- Hood, A.v.S., Wallace, M.W., and Drysdale, R.N. (2011) Neoproterozoic aragonite-dolomite seas? Widespread marine dolomite precipitation in Cryogenian reef complexes. *Geology*, 9, 871–874.
- Hu, X., Grossie, D.A., and Higgins, S. (2005) Growth and dissolution kinetics at the dolomite-water interface: An in-situ scanning probe microscopy study. *American Mineralogist*, 90, 963–968.
- Hu, X., Joshi, P., Mukhopadhyay, S.M., and Higgins, S.R. (2006) X-ray photoelectron spectroscopic studies of dolomite surfaces exposed to undersaturated and supersaturated aqueous solutions. *Geochimica et Cosmochimica Acta*, 70, 3342–3350.
- Jiang, J., Gao, M.R., Qiu, Y.H., and Yu, S.H. (2010) Gram-scale, low-cost, rapid synthesis of highly stable Mg-ACC nanoparticles and their long-term preservation. *Nanoscale*, 2, 2358–2361.
- Johnson, P.F., and Mehl, R.F. (1939) Reaction kinetics in processes of nucleation and growth. *American Institute of Mining Engineering, Technical Publication*, 1089, 1–27.
- Jones, B.F. (1965) The hydrology and mineralogy of Deep Springs Lake, California. U.S. Geological Survey of Professional Paper 502-A, 56.
- Kaczmarek, S.E., and Sibley, D.F. (2007) A comparison of nanometer-scale growth and dissolution features on natural and synthetic dolomite crystals: Implications for the origin of dolomite. *Journal of Sedimentary Research*, 77, 424–432.
- Katz, A., and Matthews, A. (1977) The dolomitization of CaCO<sub>3</sub>: An experimental study at 252–295 °C. *Geochimica et Cosmochimica Acta*, 41, 297–308.
- Keith, H.D., and Padden, F.J. Jr. (1963) A phenomenological theory of spherulitic crystallization. *Journal of Applied Physics*, 34, 2409–2421.
- Kelleher, J.J., and Redfern, S.A.T. (2002) Hydrous calcium magnesium carbonate, a possible precursor to the formation of sedimentary dolomite. *Molecular Simulations*, 28, 557–572.
- Kenward, P.A., Goldstein, R.H., González, L.A., and Roberts, J.A. (2009) Precipitation of low-temperature dolomite from an anaerobic microbial consortium: The role of methanogenic Archaea. *Geobiology*, 7, 556–565.
- Koga, N., and Yamane, Y. (2008) Thermal behaviors of amorphous calcium carbonates prepared in aqueous and ethanol media. *Journal of Thermal Analysis and Calorimetry*, 94, 379–387.
- Koga, N., Nakagoe, Y., and Tanaka, H. (1998) Crystallization of amorphous calcium carbonate. *Thermochimica Acta*, 318, 239–244.
- Land, L.S. (1998) Failure to precipitate dolomite at 25 °C from dilute solution despite 1000-fold oversaturation after 32 years. *Aquatic Geochemistry*, 4, 361–368.
- Last, W.M., and De Deckker, P. (1990) Modern and Holocene carbonate sedimentology of two volcanic maar lakes in southern Australia. *Sedimentology*, 37, 967–981.
- Lindtke, J., Ziegenbalg, S.B., Brunner, B., Rouchy, J.M., Pierre, C., and Peckmann, J. (2011) Authigenesis of native sulphur and dolomite in a lacustrine evaporitic setting (Hellin basin, Late Miocene, SE Spain). *Geological Magazine*, 148,

- 655–669.
- Lofgren, G. (1971) Spherulitic textures in glassy and crystalline rocks. *Journal of Geophysical Research*, 76, 5635–5648.
- Lothe, E., Wilson, R.M., Seshadri, R., and Meldrum, F.C. (2003) The role of magnesium in stabilising amorphous calcium carbonate and controlling calcite morphologies. *Journal of Crystal Growth*, 254, 206–218.
- Machel, H.G. (2004) Concepts and models of dolomitization: A critical reappraisal. Geological Society, London, Special Publications, 235, 7–63.
- Malone, J.M., Baker, P.A., and Burns, S.J. (1996) Recrystallization of dolomite: An experimental study from 50–200 °C. *Geochimica et Cosmochimica Acta*, 60, 2189–2207.
- Meister, P., Reyes, C., Beaumont, W., Rincon, M., Collins, L., Berelson, W., Stott, L., Corsetti, F., and Nealon, K.H. (2011) Calcium and magnesium-limited dolomite precipitation at Deep Springs Lake, California. *Sedimentology*, 58, 1810–1830.
- MacKenzie, F.T., and Andersson, A.J. (2013) The marine carbon system and ocean acidification during Phanerozoic time. *Geochemical Perspectives*, 2, 1–227.
- McKenzie, J.A., and Vasconcelos, C. (2009) Dolomite Mountains and the origin of the dolomite rock of which they mainly consist: Historical developments and new perspectives. *Sedimentology*, 56, 205–219.
- Meister, P., Gutjahr, M., Frank, M., Bernasconi, S.M., Vasconcelos, C., and McKenzie, J.A. (2011) Dolomite formation within the methanogenic zone induced by tectonically driven fluids in the Peru accretionary prism. *Geology*, 39, 563–566.
- Michel, F.M., MacDonald, J., Feng, J., Phillips, B.L., Ehm, L., Tarabrella, C., Parise, J.B., and Reeder, R.J. (2008) Structural characteristics of synthetic amorphous calcium carbonate. *Chemistry of Materials*, 20, 4720–4728.
- Miura, N., and Kawabe, I. (2000) Dolomitization of limestone with MgCl<sub>2</sub> solution at 150 °C: Preserved original signatures of rare earth elements and yttrium as marine limestone. *Geochemical Journal*, 34, 223–227.
- Nordeng, S.H., and Sibley, D.F. (1994) Dolomite stoichiometry and Ostwald step rule. *Geochimica et Cosmochimica Acta*, 58, 191–196.
- Ogino, T., Suzuki, T., and Sawada, K. (1990) The rate and mechanism of polymorphic transformation of calcium carbonate in water. *Journal of Crystal Growth*, 100, 159–167.
- Ohde, S., and Kitano, Y. (1978) Synthesis of protodolomite from aqueous solution at normal temperature and pressure. *Geochemical Journal*, 12, 115–119.
- Parkhurst, D.L. (1995) User's guide to PHREEQC—A computer program for speciation, reaction-path, advective-transport, and inverse geochemical calculations. U.S. Geological Survey Water-Resources Investigations Report 95-4227, 143 p.
- Radha, A.V., Forbes, T.Z., Killian, C.E., Gilbert, P.U.P.A., and Navrotsky, A. (2010) Transformation and crystallization energetics of synthetic and biogenic amorphous calcium carbonate. *Proceedings of the National Academy of Sciences*, 107, 16438–16443.
- Radha, A.V., Fernandez-Martinez, A., Hu, Y., Jun, Y.S., Waychunas, G.A., and Navrotsky, A. (2012) Energetic and structural studies of amorphous Ca<sub>1-x</sub>Mg<sub>x</sub>CO<sub>3</sub>·nH<sub>2</sub>O (0 ≤ x ≤ 1). *Geochimica et Cosmochimica Acta*, 90, 83–95.
- Raiteri, P., and Gale, J.D. (2010) Water is the key to nonclassical nucleation of amorphous calcium carbonate. *Journal of the American Chemical Society*, 132, 17623–17634.
- Raz, S., Hamilton, P.C., Wilt, F.H., Weiner, S., and Addadi, L. (2003) The transient phase of amorphous calcium carbonate in sea urchin larval spicules: The involvement of proteins and magnesium ions in its formation and stabilization. *Advanced Functional Materials*, 13, 480–486.
- Reddy, M.M., and Nancollas, G.H. (1976) The crystallization of calcium carbonate IV. The effect of magnesium, strontium and sulfate ions. *Journal of Crystal Growth*, 35, 33–38.
- Robie, R.A., Hemingway, B.S., and Fisher, J.R. (1978) Thermodynamic properties of minerals and related substances. U.S. Geological Survey Bulletin 1542. U.S. Government Printing Office, Washington, D.C.
- Rodriguez-Blanco, J.D., Shaw, S., and Benning, L.G. (2008) How to make “stable” ACC: Protocol and preliminary structural characterization. *Mineralogical Magazine*, 72, 283–286.
- (2011) The kinetics and mechanisms of amorphous calcium carbonate (ACC) crystallization to calcite, via vaterite. *Nanoscale*, 3, 265–271.
- Rodriguez-Blanco, J.D., Bots, P., Roncal-Herrero, T., Shaw, S., and Benning, L.G. (2012) The role of pH and Mg on the stability and crystallization of amorphous calcium carbonate. *Journal of Alloys and Compounds*, 536, Suppl. 1, S477–S479.
- Rodriguez-Blanco, J.D., Shaw, S., Bots, P., Roncal-Herrero, T., and Benning, L.G. (2014) The role of Mg in the crystallization of monohydrocalcite. *Geochimica et Cosmochimica Acta*, 127, 204–220.
- Sánchez-Román, M., McKenzie, J.A., Wagener, A.L.R., Romanek, C.S., Sánchez-Navas, A., and Vasconcelos, C. (2011) Experimentally determined biomediated Sr partition coefficient for dolomite: Significance and implication for natural dolomite. *Geochimica et Cosmochimica Acta*, 75, 887–904.
- Sand, K.K., Rodriguez-Blanco, J.D., Makovicky, E., Benning, L.G., and Stipp, S.L.S. (2012) Crystallization of CaCO<sub>3</sub> in water-alcohol mixtures: Spherulitic growth, polymorph stabilization and morphology change. *Crystal Growth and Design*, 12, 842–853.
- Sandberg, P.A. (1983) An oscillating trend in Phanerozoic non-skeletal carbonate mineralogy. *Nature*, 305, 19–22.
- Scherrer, P. (1918) Estimation of the size and internal structure of colloidal particles by means of Röntgen. *Nachrichten von der Georg-Augusts-Universität und der Königl. Gesellschaft der Wissenschaften zu Göttingen*, 2, 96–100.
- Schmidt, M., Xefliide, S., Botz, R., and Mann, S. (2005) Oxygen isotope fractionation during synthesis of CaMg-carbonate and implications for sedimentary dolomite format. *Geochimica et Cosmochimica Acta*, 69, 4665–4674.
- Shaw, S., Pepper, S.E., Bryan, N.D., and Livens, F.R. (2005) The kinetics and mechanisms of goethite and hematite crystallization under alkaline conditions, and in the presence of phosphate. *American Mineralogist*, 90, 1852–1860.
- Shtukenberg, A.G., Punin, Y.O., Gunn, E., and Kahr, B. (2012) Spherulites. *Chemical Reviews*, 112, 1805–1838.
- Sibley, D.F., Nordeng, S.H., and Borkowski, M.L. (1994) Dolomitization kinetics in hydrothermal bombs and natural settings. *Journal of Sedimentary Research*, A, 64, 630–637.
- Tracy, S.L., François, C.J.P., and Jennings, H.M. (1998a) The growth of calcite spherulites from solution I. Experimental design techniques. *Journal of Crystal Growth*, 193, 374–381.
- Tracy, S.L., Williams, D.A., and Jennings, H.M. (1998b) The growth of calcite spherulites from solution II. Kinetics of formation. *Journal of Crystal Growth*, 193, 382–388.
- Tucker, E.M., and Wright, V.P. (1990) *Carbonate Sedimentology*. Blackwell Scientific Publications, Oxford, 482 p.
- Wang, D., Wallace, A.F., De Yoreo, J.J., and Dove, P.M. (2009) Carboxylated molecules regulate magnesium content of amorphous calcium carbonates during calcification. *Proceedings of the National Academy of Sciences*, 106, 21511–21516.
- Warthmann, R., van Lith, Y., Vasconcelos, C., McKenzie, J.A., and Karpoff, A.M. (2000) Bacterially induced dolomite precipitation in anoxic culture experiments. *Geology*, 28, 1091–1094.
- White, W.B. (1974) The carbonate minerals. In V.C. Farmer, Ed., *The Infrared Spectra of Minerals*. London, Mineralogical Society Monograph 4, pp. 227–284.
- Zempolich, W.G., and Baker, P.A. (1993) Experimental and natural mimetic dolomitization of aragonite ooids. *Journal of Sedimentary Petrology*, 63, 596–606.
- Zhang, F., Xu, H., Konishi, H., Shelobolina, E.S., and Roden, E.E. (2012) Polysaccharide-catalyzed nucleation and growth of disordered dolomite—A potential precursor of sedimentary dolomite. *American Mineralogist*, 97, 556–567.

MANUSCRIPT RECEIVED MARCH 7, 2014

MANUSCRIPT ACCEPTED OCTOBER 29, 2014

MANUSCRIPT HANDLED BY SIMON REDFERN